Biosensors and Bioelectronics 142 (2019) 111549

Contents lists available at ScienceDirect

Biosensors and Bioelectronics

journal homepage: www.elsevier.com/locate/bios

Efficient electron-mediated electrochemical biosensor of gold wire for the rapid detection of C-reactive protein: A predictive strategy for heart failure

A.T. Ezhil Vilian[a], Wonyoung Kim[b], Bumjun Park[c], Seo Yeong Oh[c], TaeYoung Kim[b], Yun Suk Huh[c,*], Chang Kwon Hwangbo[b,**], Young-Kyu Han[a,***]

[a] Department of Energy and Materials Engineering, Dongguk University-Seoul, Seoul, 100-715, Republic of Korea
[b] Department of Physics, Inha University, 100 Inha-ro, Michuhol-gu, Incheon, 22212, Republic of Korea
[c] Department of Biological Engineering, Inha University, 100 Inha-ro, Michuhol-gu, Incheon, 22212, Republic of Korea

ARTICLE INFO

Keywords:
Gold wires
C-reactive protein
Immunosensor
Electrochemical detection
Square wave voltammetry

ABSTRACT

C-reactive protein (CRP) is considered a promising biomarker for the rapid and high-throughput real-time monitoring of cardiovascular disease and inflammation in unprocessed clinical samples. Implementation of this monitoring would enable various transformative biomedical applications. We have fabricated a highly specific sensor chip to detect CRP with a detection limit of 2.25 fg/mL. The protein was immobilized on top of a gold (Au) wire/polycarbonate (PC) substrate using 1-ethyl-3-(3-dimethylamino-propyl) carbodiimide hydrochloride/N-hydroxy succinimide-activated 3-mercaptoproponic acid (MPA) as a self-assembled monolayer agent and bovine serum albumin (BSA) as a blocking agent. In contrast to the bare PC substrate, the CRP/BSA/anti-CRP/MPA/Au substrate exhibited a considerably high electrochemical signal toward CRP. The influence of the experimental parameters on CRP detection was assessed via various analysis methods, and these parameters were then optimized. The linear dynamic range of the CRP was 5–220 fg/mL for voltammetric and impedance analysis. Morever, the strategy exhibited high selectivity against various potential interfering species and was capable of directly probing trace amounts of the target CRP in human serum with excellent selectivity. The analytical assay based on the CRP/BSA/anti-CRP/MPA/Au substrate could be exploited as a potentially useful tool for detecting CRP in clinical samples.

1. Introduction

C-reactive protein (CRP) is widely accepted as a diagnostic biomarker used for monitoring cardiovascular disease and inflammation and is well known as an acute-phase protein, which is mainly synthesized by the liver (Kuo et al., 2018; Wongkaew et al., 2018). The concentration of normal plasma CRP is below 1.0 mg L^{-1}, and the clinical diagnostic level ranges from 1 to 3 mg L^{-1} in healthy humans (Bryan et al., 2013; Cai et al., 2018; Kowalczyk et al., 2018). Many diseases, such as cardiovascular and inflammatory diseases, are mainly caused by a high level of CRP in plasma (Wang et al. 2014, 2017; Zhou et al., 2014). Consequently, an early, accurate, and highly sensitive analytical methodology/sensory system for the sensing of CRP plays a crucial role in clinical carcinoma diagnosis and pharmaceutical research (Chen et al., 2017). In clinical laboratories, many analytical assays, including enzyme-linked immunoassay (ELISA), turbidimetry, and nephelometry, have been employed in the last few decades to detect CRP in human serum (Salminen et al., 2018; Lee et al., 2018; Turner, 2013; Zhang et al., 2019). However, these previously existing methods for clinical practice have limitations such as high-cost, low sensitivity, time-consuming and error prone (Letchumanan et al., 2019; Cheen et al., 2017; Suginta et al., 2013).The ideal CRP detection technique should be of high sensitivity, reproducible, simple, specific, and user-friendly in the clinical setting (Vigushin et al., 1993). Various methods for CRP detection in biological samples, including surface plasmon resonance (SPR), piezoelectric microcantilevers, quartz crystal microbalance technology, microfluidics, and electrochemical sensors, have been employed (Hu et al., 2006; Lemos et al., 2017; Lee et al., 2011). However, these techniques are time-consuming, expensive, prone to errors, lack of sensitive (limit of detection ca. 0.1 mg L^{-1}), and require skilled personnel, complex operation processes, and sophisticated equipment (Kitayama and Takeuchi, 2014). Thus, an ultrasensitive and highly

* Corresponding author.
** Corresponding author.
*** Corresponding author.
E-mail addresses: yunsuk.huh@inha.ac.kr (Y.S. Huh), hwangbo@inha.ac.kr (C.K. Hwangbo), ykenergy@dongguk.edu (Y.-K. Han).

https://doi.org/10.1016/j.bios.2019.111549
Received 13 April 2019; Received in revised form 26 July 2019; Accepted 28 July 2019
Available online 31 July 2019
0956-5663/

selective method for the rapid and quantitative determination of trace CRP levels is required (Vashist et al., 2016). Electrochemical techniques represent the most promising methods in terms of low price, small sample volume, high sensitivity, wide dynamic concentration response range, and versatility (Songjaroen et al., 2016). Therefore, numerous attempts have been made to construct electrochemical immunosensors for detecting CRP and to overcome the shortcomings of conventional assays (Thangamuthu et al., 2018).

Many nanomaterials have been used as suitable electrode materials for immobilization of biomolecules or as signal molecules for improving the sensitivity of CRP immunosensors (Dorraki et al., 2018). These nanomaterials include metal nanoparticles (such as Au, Bi, and Hg), quantum dots, poly(dimethylsiloxane)-gold nanoparticle composites, vertically aligned carbon nanofibers with generated carboxylic acid groups, and composites of polyaniline with molybdenum disulfide (Dong et al., 2019a,b; Gupta et al., 2014; Zhang et al., 2016; Zhou et al., 2010). However, some of these materials fail to meet the criteria for application as nanomaterials due to the multiple preparation steps required, the toxicity of the heavy metal nanoparticles, and low sensitivity (Dong et al., 2019a,b). Many methods can be employed to improve the applicability of these materials. These include simplification of the biosensor construction, application of non-toxic elements, and the design of new ultra-sensitive, rapid-response, reliable, and label-free sensors for electrochemical detection of CRP (Kokkinos et al., 2015). Microchips and bio substrates have been fabricated (through miniaturized technologies) and widely applied for gene and protein analyses mainly due to their high-throughput, ease of operation, and excellent reliability (Chen et al., 2012). In environmental and food monitoring, miniaturization holds excellent promise for on-site monitoring and detection (Jarczewska et al., 2018). Chip-based sensors are technically compatible with miniaturization technologies (Johnson et al., 2004). Several chip-based methods, including polymer matrices, oligopeptide-modified silicon nanowires, DNAzyme, proteins, and oligonucleotides, have been used for CRP analyses (Matsuura et al., 2016; Dong et al., 2019a,b; Vilian et al., 2019; Wang et al., 2017a,b). To enhance the sensitivity of the electrochemical aptasensors, Au nanoparticles (Au NPs) are used as the amplifying element due to their large surface area, rapid electron transfer, efficient electrocatalytic properties, and excellent biocompatibility, particularly when deposited on polymer support (Mohammed and Desmulliez, 2011). Compared with the single-component nanoparticles, these NPs exhibit superior performance in terms of catalytic activity, due to the synergetic effect at the metal/polymer support interface, which can also provide more active sites (Lee et al., 2010).

Many researchers have developed approaches that yield nanostructured materials with one-dimensional linear (nanotube, nanowire, nanorod, nanofiber or nanobelt) morphologies, as well as two-dimensional and hierarchical three-dimensional sheets (Xie et al., 2012). Among these morphologies, nanowires have recently received considerable attention due to their unique properties and, in turn, significant potential for application in a wide range of materials and technologies for biomedical engineering (Liu et al., 2019; Li et al., 2015). Until now, researchers have applied one-dimensional nanostructures to (for example) biochemical applications, electronic devices, photonics, and sensors. Therefore, several approaches for nanowire fabrication have been reported (McAlpine et al., 2007). Most nanowire fabrication techniques used are chemically based synthetic methods (Zhang et al., 2017). The vapor-state reactions and electrochemical growth of metal nanowires through porous membrane templates have used solution-based nanowire growth of silver (Ag) or zinc oxide (ZnO) and the generation of nanowires (Im et al., 2006). Top-down fabrication approaches have also been used to create nanowires via (typically) lithographic patterning techniques (Thurn-Albrecht et al., 2000). To date, many researchers have proposed new approaches and have obtained extremely long nanowires (length of millimeters and centimeters) with excellent uniformity of crystals, high electrical conductivity, and versatility of materials (Xing et al., 2003). Despite these excellent properties, predictable alignment of the nanowires for applications and reliable device fabrication remains challenging (Sun et al., 2002). The use of ultralong and large-area nanograting templates have allowed the development of rapid and effective fabrication techniques that achieve highly ordered nanowire arrays composed of various materials (Zubiate et al., 2017). For example, metal nanowire arrays of a wire grid polarizer have been developed for use in biological applications.

Herein, we designed a simple and ultrasensitive sandwich-type electrochemical immunosensor for the detection of CRP in human serum samples. Gold (Au) nanowires grown on PC substrate were used as an efficient biosensor platform for anchoring anti-CRP antibody (anti-CRP) to detect CRP which enhances the electrochemical signal of the immunosensor. We believe that the proposed immunosensor demonstrates admirable linear range, a low detection limit, featuring reliable selectivity, high sensitivity, good reproducibility, reusability, and acceptable stability. Thus, the fabricated immunosensor is expected to be applied in clinical analyses for the accurate quantitative detection of CRP in human serum samples. It gives an opportunity for the early diagnosis of cancer, and prognosis monitoring of diseases.

2. Experimental section

2.1. Materials

Bovine serum albumin (BSA), 1, 1-ethyl-3-(3-dimethylaminopropyl) carbodiimide hydrochloride (EDC), N-hydroxy succinimide (NHS), 3-mercaptopropionic acid (MPA), and potassium hexacyanoferrate, potassium hexacyanoferrate trihydrate, prostate-specific antigen (PSA), dopamine (DA), lysine (Lys), uric acid (UA), L-cystine (L-Cys), glutathione (GSH), histidine (His), serine (Ser), carcinoembryonic antigen (CEA), human chorionic gonadotrophin (HCG), glycine (Gly), and glucose were ordered from Sigma-Aldrich Corporation. C-reactive protein (CRP) antigen and antibody (anti-CRP) were provided by Sigma-Aldrich. The capture and signaling anti-CRP stock solutions (100 μM) and phosphate buffer saline solutions (PBS, pH 7.0) were prepared in ultra-pure double distilled water ($\geq$18.2 MΩ cm) generated by a Barnstead Easypure System (Thermo Scientific Inc., Dubuque, USA). Phosphate buffer saline (PBS, pH 7.0) was prepared using KCl, Na_2HPO_4 and NaH_2PO_4.The solutions were kept frozen in a freezer at −10 °C until use. All other chemicals and reagents were obtained in analytical grade and used as-received without further purification. The electrolyte was purged for 15 min with high-purity nitrogen prior to each electrochemical measurement.

2.2. Apparatus

The morphology of the Au/PC substrate was observed via scanning electron microscopy (SEM; Hitachi SU 8010, Japan). X-ray diffraction (XRD) patterns of the prepared samples were recorded by using an X'Pert PRO MRD (Phillips) X-ray diffractometer equipped with a CuKα radiation source ($\lambda = 1.54056$ Å, 2θ scanning rate: $0.02^{\circ}\ s^{-1}$). Fourier transform infrared (FTIR) spectra were recorded and X-ray photoelectron spectroscopy (XPS) analyses were performed on a Bruker VECTOR 22 spectrometer using the KBr pellet technique and a Thermo scientific K-Alpha system, respectively. Electrochemical measurements were conducted using an AUTOLAB PGSTAT 302N Electrochemical Workstation (Metrohm Autolab b.v., Herisau, Switzerland) with a three-electrode system consisting of an Ag/AgCl (3 M KCl) reference electrode, Pt wire counter electrode, and a BSA/anti-CRP/MPA/Au substrate working electrode. Electrochemical experiments were performed in 5 mM $[Fe(CN)_6]^{3-/4-}$ prepared in PBS buffer (pH 7.0, containing 0.1 M KCl) via square wave voltammetry (SWV; the amplitude of signal: 40 mV, frequency: 60 Hz) at potentials ranging from −0.30–0.90 V versus Ag/AgCl references.

2.3. Preparation of the Au substrate

A facile route for the fabrication of nanowire arrays of an Au wire grid polarizer was demonstrated using nanoimprint lithography and oblique angle deposition methods. A PC sheet was employed as the substrate (Kim et al., 2018; Yeon et al., 2013). Moreover, a PC solution was first coated on a Si mold and the curing process, which was realized via UV irradiation, resulted in a crosslinked PC. Au structures were deposited on nanopatterned polymers using an oblique angle deposition method in a customized electron beam evaporator (DIAD-700-customized model, Daeryung Vacuum Co. Ltd., Korea) (Kim et al., 2019; Lakhtakia and Messier, 2005). The Au metal vapor was deposited at a rate of 0.5 nm/s on top of the nano-patterned polymer substrate at a tilt angle of 50°. The serial bi-deposition method was implemented, where the Au metal vapor was deposited at 0.5 nm/s whenever the substrate holder was rotating periodically at 180°. A 20-nm-thick Au film was first deposited on the top of the nanopatterned polymer substrate. The shutter was then closed to rotate the substrate at an angle of 180° and the second deposition was performed for another 20-nm-thick Au.

2.4. Immunosensor preparation

The Au/PC substrate was dipped in 10 µL MPA (10 mM) prepared in double distilled water at 20 °C for 30 min. Afterward, the substrate was rinsed with ultrapure water, via ultra-sonication, to remove the unbound MPA residue from the surface. Subsequently, a 30 mM EDC and 2 mM NHS solution was pumped into the MES solution to activate the COOH-terminated group of MPA. The MPA-modified Au substrate (MPA/Au substrate) was then immersed in a 1 mL 20 mM MES solution (pH 4.6) for 12 h. Subsequently, a 20 µL aliquot of 0.1 mg/mL anti-CRP antibody was conjugated to the EDC/NHS-activated MPA/Au substrate at room temperature for 4 h and rinsed with PBS. To prevent non-specific adsorption and passivation at the electrode surface, the anti-CRP/EDC/NHS-activated MPA/Au substrate was then incubated with 1% (w/v) BSA for 2 h. A small amount (20 µL) of a buffer solution containing the appropriate concentration of CRP samples was coated for 30 min on the electrode surface at room temperature. The surface was then rinsed with PBS. Changes in the electrochemical performance of the electrode/electrolyte interface were investigated via cyclic voltammetry (CV) and electrochemical impedance spectroscopy (EIS). The procedure for assembling the immunosensor is shown in Scheme 1.

3. Results and discussion

3.1. Characterization of Au substrate

Scanning electron micrographs obtained at various magnifications (Fig. 1a–d) showed that the Au nanowire was grown along the PC substrate, indicative of Au nanowire formation on the substrate surface. The top view SEM images allow 3D visualization of these Au nanowires and PC substrate (Fig. 1a–b and Figs. S1a–b). The cross-sectional view revealed that the nanowires were first cast on PC boards and immobilized to form vertical nanowires. In the present study, successful Au modifications of PC substrates were identified via FTIR spectroscopy. In the spectrum obtained for the pure PC substrate (see Fig. 2a), the bands occurring at: 1192 cm^{-1} and 1745 cm^{-1}, 1155 cm^{-1} and 1230 cm^{-1}, 2975 cm^{-1}, 1500 cm^{-1}, and 862 cm^{-1} are attributed to –C=O stretching vibrations, C–O bending vibrations, $–CH_3$ stretching vibrations, C=C bonds of the aromatic ring, and C–C bond stretching (Baik et al., 2017; Yuan et al., 2018), respectively. After modification with Au, the characteristic band of the –C=O stretching vibration bound to Au shifts to 1745 cm^{-1}. These results showed that Au was successfully attached to the surface of the PC substrate. The crystalline structure and phase purity of the Au substrate was determined via XRD pattern analysis (Fig. 2b). A broad diffraction peak centered at 18.5° occurs in the XRD pattern of the pure PC substrate. The peaks were diffuse, indicating the amorphous nature of the material. For the Au/PC substrate, the highest intensity diffraction peaks occurred at 39.21°, 45.59°, 66.33°, and 79.78° corresponding to the (111), (200), (220), and (311) planes, respectively (JCPDS card: no. 004–0784) (Hühn et al., 2016). The XRD pattern revealed that the Au nanowires were successfully integrated into the surface of the PC substrate. The chemical composition characteristics of the Au substrate were evaluated via XPS. As shown in Fig. 2c, the substrate contained only C, Au, and O elements. The corresponding C1s spectra consisted of five distinct peaks. These occurred at 284.6, 285.2, 286.8, 290.2, and 290.7 eV, which correspond to aromatic C–H, aliphatic C–H, C–O, aromatic O=C–O bands, and π-π* shake up satellites, respectively (Fig. 2d). The corresponding O 1s spectra peaks are located at 533.70, 564.12, and 532.32 eV. The Au $4f_{7/2}$ peak and the Au $4f_{5/2}$ peak were associated with binding energies of 83.93 and 87.71 eV, respectively, confirming the successful deposition of gold onto the PC substrate surfaces (Fig. 2e).

3.2. Electrochemical investigation of the sensor

Each modification step comprising the CRP/BSA/anti-CRP/MPA/Au substrate construction process in 5 mM $[Fe(CN)_6]^{3-/4-}$ prepared in PBS buffer (pH 7.0, containing 0.1 M KCl) was verified via CV experiments

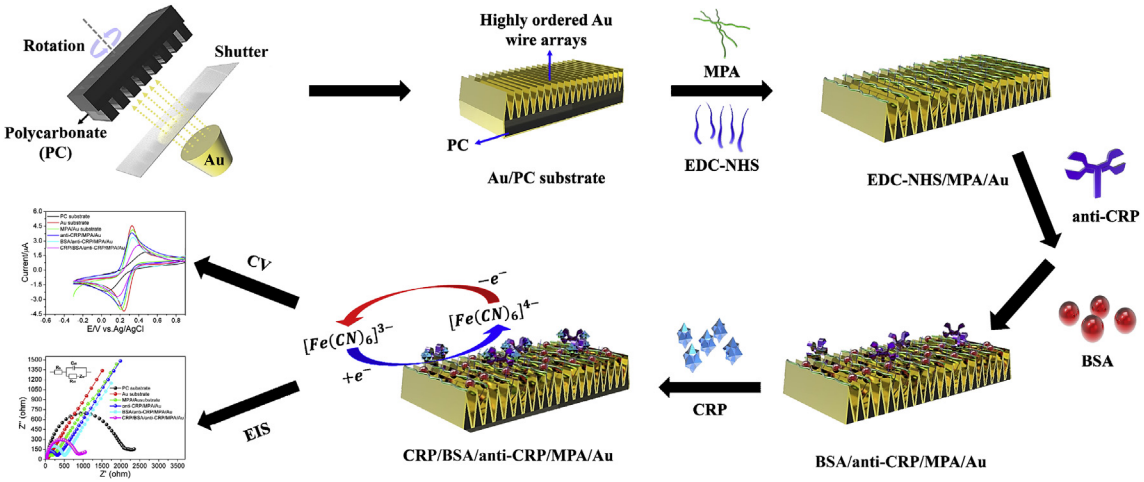

Scheme 1. (a) Schematic showing the fabrication of the CRP/BSA/anti-CRP/MPA/Au substrate.

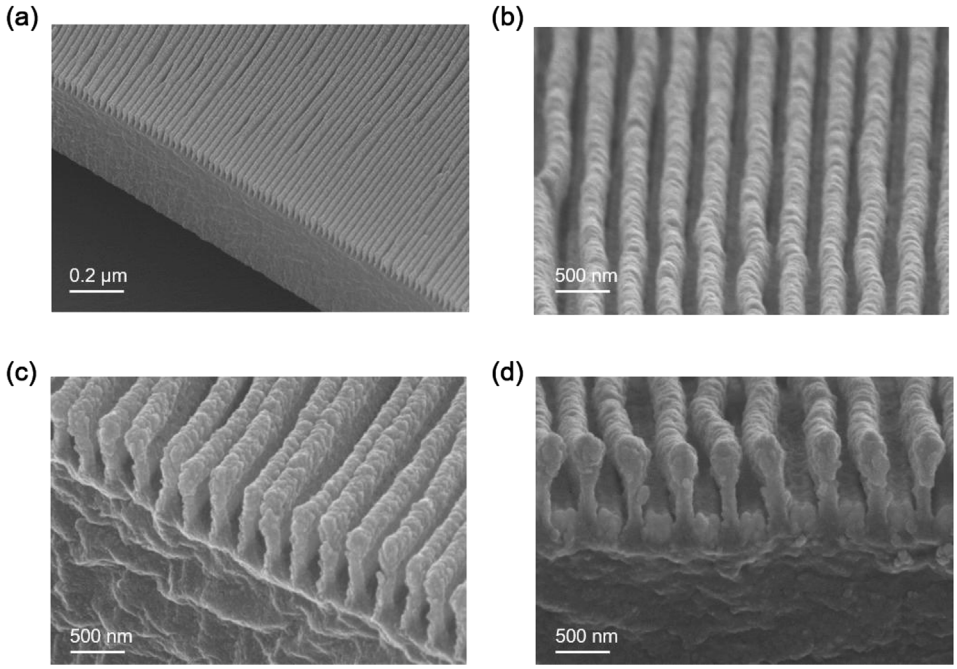

Fig. 1. (a–d) Scanning electron micrographs obtained at various magnifications of the Au/PC substrate.

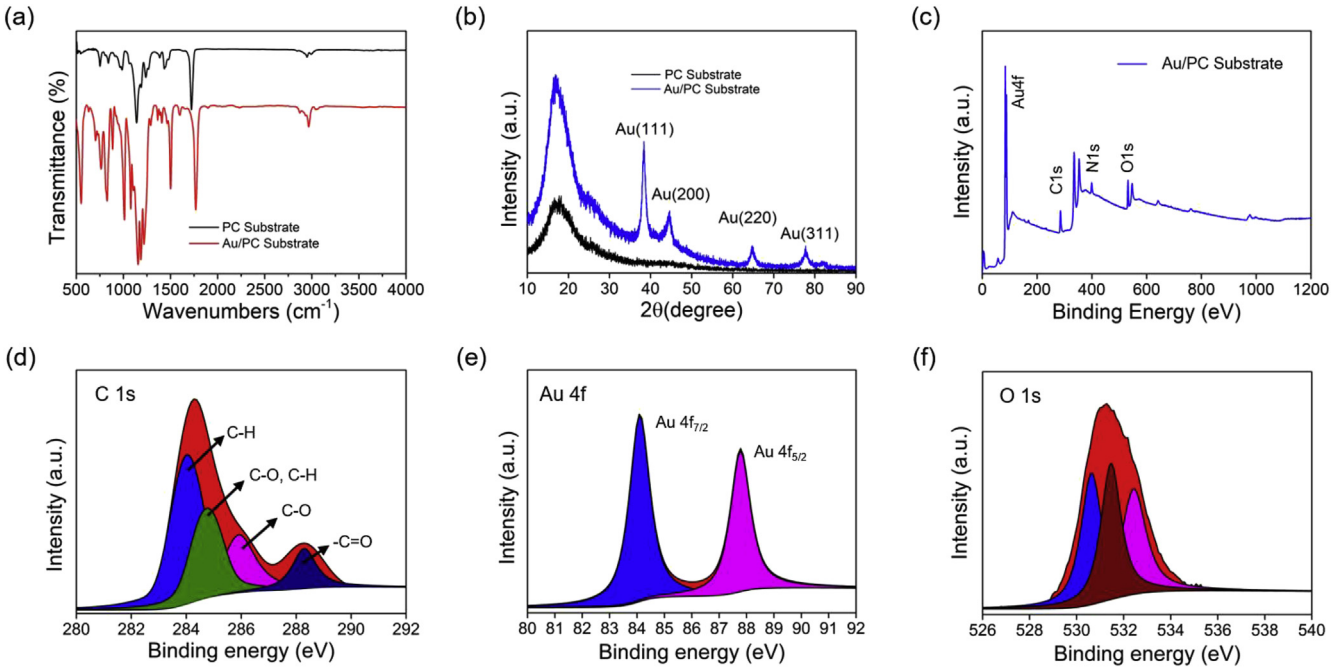

Fig. 2. (a) FTIR spectra of the PC substrate and Au substrate, (b) XRD patterns of the Au substrate and PC substrate, (c) XPS survey spectrum of the Au/PC substrate, high-resolution XPS spectra of (d) C 1s, (e) Au 4f, and (f) O 1s of the Au/PC substrate.

(see Fig. 3a). The peak current measured on the PC substrate led to a decrease in the quasi-redox peak currents and a considerable increase in the resistance. The redox peak currents of the Au-modified PC substrate were relatively high, suggesting that the Au substrate had a high surface area, compatible ambience, good conductivity, and distinctive electron transfer capacity. It has been observed from Fig. 3a, the peak current of the Au substrate was decreased along with increased peak potential separation (ΔE_p) after modification with MPA, which may be due to the hindrance of electron transfer from the electrolyte to the surface of Au substrate by MPA (Chen et al., 2008; Johari-Ahar et al., 2015).When the anti-CRP was coupled to the MPA/Au substrate, an extremely low peak current was maintained, and the difference between the redox peak potentials became large. Subsequently, the anti-CRP/MPA/Au substrate was blocked with BSA to prevent non-specific adsorption on the anti-CRP/MPA/Au substrate surface. This weak response may have resulted from the electronically inert characteristics of BSA and anti-CRP. After capturing the target CRP, the peak current decreased further. Afterward, the BSA/anti-CRP/MPA/Au substrate was incubated with CRP. The peak currents decreased slightly, owing to the electron-blocking layer, thereby hindering the efficient electron transfer behavior of the CRP.

The assembly processes comprising the CRP/BSA/anti-CRP/MPA/

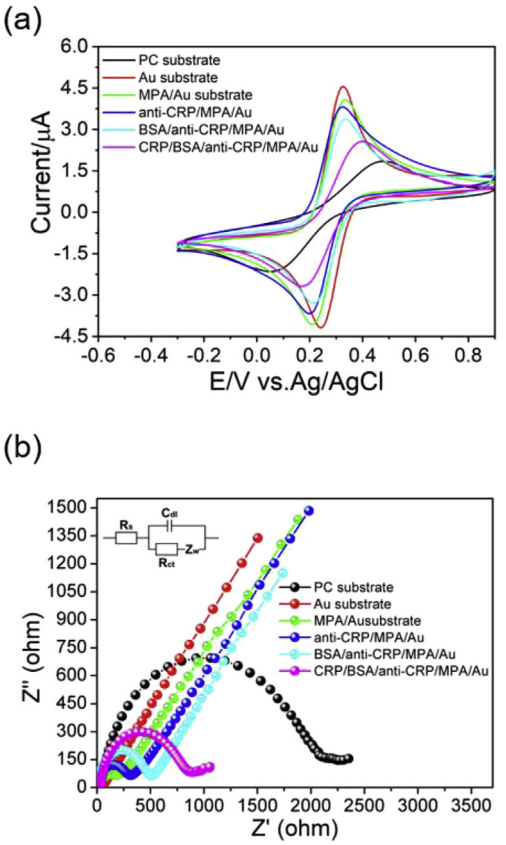

Fig. 3. (a) Cyclic voltammetry (CV) curves and (b) electrochemical impedance spectra obtained in 0.1 M KCl solution containing an equimolar (5 mM) mixture of $K_3Fe(CN)_6$ and $K_4Fe(CN)_6$ at the PC substrate, Au substrate, MPA/Au substrate, anti-CRP/MPA/Au substrate, BSA/anti-CRP/MPA/Au substrate, and CRP/BSA/anti-CRP/MPA/Au substrate. Inset: Randel's circuit model.

Au substrate construction process were evaluated via EIS, and the resulting Nyquist plot consisted of a straight linear region and a semicircular region. The electron transfer rate of the redox probe on the substrate surface was controlled by the electron transfer resistance (R_{ct}) equal to the semicircular diameter. As shown in Fig. 3b, the Nyquist plot of the PC substrate is characterized by a large semicircle diameter (2183 Ω). Due to its excellent conductivity, when Au was immobilized on the substrate (80 Ω), the diameter of the semicircle became smaller than that of the substrate. This indicated that the electron transfer of $[Fe(CN)_6]^{3-/4-}$ on the substrate surface was improved. It is observed that R_{ct} value is increased for MPA/Au substrate (307 Ω) due to the formation of insulating film layer which hinders the electron conduction from the electrolyte to the Au substrate surface and resulted in the increased electron transfer resistance. After incubation of the MPA/Au in the anti-CRP solution, the semicircle diameter increased significantly (307 Ω), owing to protein blocking of the electron transfer. After BSA assembly, the semicircle diameter of the anti-CRP/MPA/Au substrate (508 Ω) increased more significantly than that of the Au substrate, suggesting that electron transfer is hindered by BSA with insufficient conductivity. The semicircle diameter changed when CRP was stabilized during BSA/anti-CRP/MPA/Au substrate construction (888 Ω).Capture antibodies (anti-CRP) specific to CRP were functionalized onto the surface of Au wire/PC substrate by using 1-ethyl-3-(3-dimethylamino-propyl) carbodiimide hydrochloride/N-hydroxy succinimide-activated 3-mercaptoproponic acid (MPA) monolayer which immobilizes BSA. The double layer capacitance (C_{dl}) and electron transfer resistance (R_{ct}) values depend on the insulating features at the Au substrate/electrolyte interface. It was observed through Randell circuit of the EIS analysis, the C_{dl} and R_{ct} values have been changed when the Au substrate was modified with the modifier which is an indirect method to detect the modifier on the Au substrate. This strategy can be utilized to detect the target CRP molecules with high sensitivity which requires the interaction of the anti-CRP at the junction between the fluid media and the substrate surface. More importantly, the results revealed that the CRP/BSA/anti-CRP/MPA/Au substrate was successfully established.

Cyclic voltammetry measurements of 5 mM $[Fe(CN)_6]^{3-/4-}$ prepared in PBS buffer (pH 7.0, containing 0.1 M KCl) were performed at scan rates of 10–100 mV/s with a standard electrochemical cell using a CRP/BSA/anti-CRP/MPA/Au substrate as the working electrode (Fig. S2a). As the resulting voltammograms show, the current response increased linearly with increasing scan rate. The electrode surface area of the CRP/BSA/anti-CRP/MPA/Au substrate was calculated from the Randle-Sevcik equation. This equation is given as $I_p = 2.69 \times 10^5 AD^{1/2} n^{3/2} \nu^{1/2} C$, where, I_p, n, A, D, C, and ν are the respective peak current (A), number of electrons, electrode area (cm^2), diffusion coefficient of the species (cm^2/s), concentration (mol/cm^3) of the species, and scan rate (V/s). Slopes of 4.394 + 2.129 μA ($R^2 = 0.9981$) and −4.501 − 0.709 μA ($R^2 = 0.9967$) for the cathodic and anodic lines, respectively, were obtained from the plot of Ip vs. ν^2 (Fig. S2b) for the standard electrochemical cell. The electrode surface area of the CRP/BSA/anti-CRP/MPA/Au substrate was 5.30 x 10^{-3} cm^2. The immunosensor using BSA/anti-CRP/MPA/Au as signal labels exhibited significantly greater electrochemical responses, owing to the following reasons: first, the Au substrate with good adsorption properties could enhance the load of anti-CRP; second, Au with excellent biocompatibility could provide sufficient adsorption groups which resulted in the increase of more CRP adsorption thereby leak out of CRP is prevented; third, Au nanowire with high electrical conductivity could facilitate electron transfer. These results indicated that CRP/BSA/anti-CRP/MPA/Au substrate exhibits reversible diffusion-controlled behavior with an electron transfer process.

3.3. Optimization of experimental parameters associated with immunosensor

The pH of PBS plays a key role in the performance of the immunosensor. For a given set of incubation conditions, the electrochemical activity of the CRP immunosensor was evaluated for pH values ranging from 5.0 to 8.5 (Fig. S3). The electrochemical probe of the CRP/BSA/anti-CRP/MPA/Au substrate exhibited an enhanced current response at a constant potential (0.23 V), associated with a relatively low current corresponding to a pH of 7.0. This indicated that more anti-CRP occurred on the surface than in the other regions. When the pH was varied (i.e., increased and decreased), the CRP and the anti-CRP in the immune complexes of the biomolecules were unstable under strongly acidic or alkaline conditions, owing to a loss in activity. This was validated by the reduction in the peak current. Therefore, a pH of 7.0 was chosen as the optimum pH value for further CRP measurements.

The effect of CRP concentration on the sensitivity of the prepared immunosensor was investigated, by evaluating the immunocomplex formation on the BSA/anti-CRP/MPA/Au substrate. When the anti-CRP concentration was increased (from 15 to 150 μg/mL), the peak current decreased and then remained constant at concentrations above 100 μg/mL (Fig. S4). This indicated that the anti-CRP on the surface of the BSA/MPA/Au substrate was sufficient for capture of the CRP. The effect of incubation time on the sensitivity of the CRP/BSA/anti-CRP/MPA/Au substrate electrochemical response signal was investigated. When the CRP reached the anti-CRP on the BSA/MPA/Au substrate surface of the immunosensor in the incubation solution, the species in contact formed immune complexes after prolonged periods (see Figs. S5 and 6). When the incubation time of the CRP was increased from 10 to 70 min, the peak current response decreased gradually and reached a stable value after 30 min. The anti-CRP and antigen CRP incubation time of 30 min indicated the saturated capture of CRP at the BSA/anti-CRP/MPA/Au

substrate surface. Moreover, the concentration of BSA had a significant effect on the electrochemical current responses of the anti-CRP/MPA/Au substrate. The corresponding background signal resulting from non-specific adsorption of CRP onto the anti-CRP/MPA/Au substrate surface can lead to poor results. To reduce the non-specific adsorption of CRP and anti-CRP on the MPA/Au substrate surface, the surface was blocked by the addition of BSA after the anti-CRP immobilization step. As shown in Fig. S7, the current response decreased sharply with increasing BSA concentration (0%–1% (w/v)) until a concentration of 0.4% (w/v) was reached. We believe that the blocking can also minimize the adsorption of non-specific CRP on the anti-CRP/MPA/Au substrate surface. Consequently, 0.4% (w/v) BSA was selected for the subsequent experiments. To obtain the best response for CRP detection, the electroanalytical parameters (including the scan rate, concentration of the aptamer, amount of BSA, and incubation time) of the experiment were optimized. All the analytical experiments were performed in triplicate. Using the calibration curve, the data were plotted by standard deviation method as error bars. The results represent the mean (standard deviation) of three independent experiments and are given in Tables S1–S5.

3.4. Analytical performance

Compared with CV analysis, the SWV technique can rapidly detect (with low detection limits, high selectivity, and high sensitivity) biomarkers associated with diseases (Thapliyal et al., 2016; Zamay et al., 2016). We recorded CRP/BSA/anti-CRP/MPA/Au substrates, for CRP concentrations ranging from 5 to 220 fg/mL (slope = $-0.0244x + 5.5002$ μA/decade, $R^2 = 0.9941$) in 5 mM $[Fe(CN)_6]^{3-/4-}$ prepared in PBS buffer (pH 7.0, containing 0.1 M KCl). As shown in Fig. 4a, the specific CRP increased gradually, while the corresponding peak current decreased gradually without significant peak shift or variation in breadth. The sensor fabricated in this study exhibited excellent electroanalysis performance, as evidenced by a detection limit of 2.25 fg/mL (3σ/slope; see Fig. 4b). Furthermore, this wide linear range and low detection limit are considerably lower than the values reported for the previous methods employing precision instruments (Table 1). The SWV results, which are comparable to the electroanalysis performance revealed by EIS, are shown in the calibration graph (Fig. 5a).

The Nyquist plots corresponding to the fabricated biosensors incubated at increasing concentrations of CRP are shown in Fig. 5a and b. The R_{ct} increased because the antigen-antibody complex formed on the surface of the biosensor leads to poor conductivity of the system. The specificity of the assay was evaluated using the CRP/BSA/anti-CRP/MPA/Au substrate, and the impedance response remained unchanged for concentrations ranging from 7 to 215 fg/mL. The corresponding linear regression was described by $\Delta R_{ct} = 15.166x + 571.06$, ($R^2 = 0.9943$). These results revealed that the fabricated biosensor has high sensitivity to the CRP assay. Impedance detection is quite suitable for clinically relevant levels of CRP and detection limits as well as quantification limits of 3 fg/mL (3σ/slope) and 0.01 fg/mL (10σ/slope), respectively, were realized. To evaluate the validity of the fabricated electrochemical sensor, the BSA/anti-CRP/MPA/Au substrate was used for the detection of CRP in 5 mM $[Fe(CN)_6]^{3-/4-}$. Error bars in the SWV and EIS calibration plots indicate the standard deviation of the electrochemical sensing performance from three repetitive measurements (n = 3). The error bars data for three repeated measurements are shown in Tables S6–S7.

3.5. Selectivity verification of the immunoensor

Selectivity represents an important feature of a biosensor. We, therefore, investigated the selectivity of the designed CRP/BSA/anti-CRP/MPA/Au substrates using SWV, an extremely selective electrochemical detection technique for trace amount analysis. Experimental

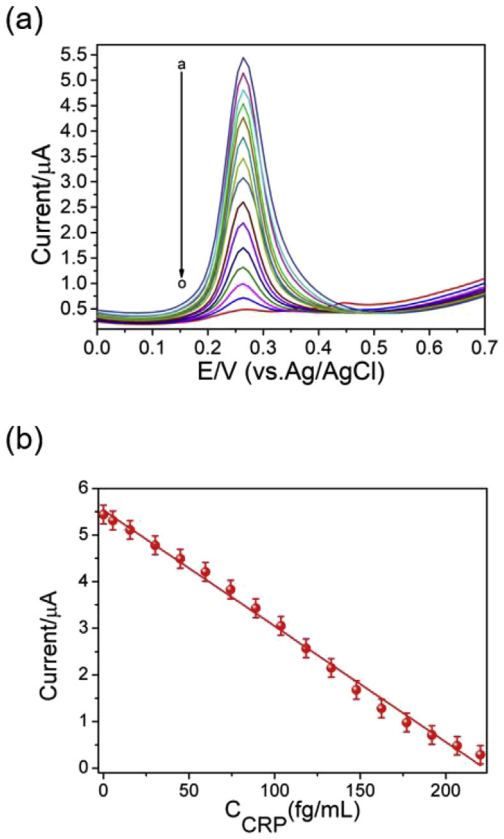

Fig. 4. (a) SWV curves of BSA/anti-CRP/MPA/Au substrate for various CRP concentration ranging from 0 to 220 fg/mL (from a to o) in 5 mM $[Fe(CN)_6]^{3-/4-}$ prepared in PBS buffer (pH 7.0, containing 0.1 M KCl) solution. (b) Calibration plot corresponding to the different concentrations of CRP vs. peak current (n = 3).

results demonstrated that a 50 fg/mL concentration of CRP in 5 mM $[Fe(CN)_6]^{3-/4-}$ prepared in PBS buffer (pH 7.0, containing 0.1 M KCl) was used to evaluate the selectivity of the sensor in the presence of different non-specific binding proteins, including prostate-specific antigen (PSA), dopamine (DA), lysine (Lys), uric acid (UA), L-cystine (L-Cys), glutathione (GSH), histidine (His), serine (Ser), carcinoembryonic antigen (CEA), human chorionic gonadotrophin (HCG), glycine (Gly), and glucose (Glu) (10 fg/mL). Although the signal fluctuated to a certain extent (Fig. S8), the current signals changed only slightly in the presence of each protein, compared with those of the blank signal corresponding to the immunosensor. These results confirmed that the developed immunosensor exhibits considerable selectivity toward CRP.

3.6. Applicability of the sensor to clinical diagnosis

For the clinical application of the proposed sensor to the early diagnosis of CRP, the sensitivity of this system should be validated in a biochemical environment similar to blood serum. First, CRP detection was performed in 5 mM $[Fe(CN)_6]^{3-/4-}$ prepared in PBS buffer (pH 7.0, containing 0.1 M KCl) solution using the prepared immunosensor based on optimal conditions (Fig. S9a). The human serum sample was diluted 100-fold with a buffer solution. These serum samples were then spiked with different concentrations of CRP (12 fg/mL-166 fg/mL) in PBS buffer solution. Moreover, SWV was used to determine the relationship between the decreased peak current values and CRP concentrations (Fig. S9b). This relationship was described by a regression equation of I (μA) = $-0.0119x + 2.2236$ (correlation coefficient: 0.9977). The CRP limit of detection was 4.5 fg/mL (S/N = 3). The result revealed that the proposed immunosensor exhibits the required electrochemical

Table 1
Analytical performance of previously reported CRP immunosensors compared with that of the sensors proposed in the current study.

Immunosensor	Analytical technique	LOD	Linear range	Ref.
GCE/PEI-Fc/Ab/CRP	EIS	2.5 (ng mL^{-1})	1x5x10^4 (ng mL^{-1})	Kowalczyk et al. (2018)
	DPV	0.5 (ng mL^{-1})	1 x5x10^4 (ng mL^{-1})	
antiCRP-SAM-AuNPs-SPE	amperometry	0.150 (nM)	0.4–200 (nM)	Thangamuthu et al. (2018)
BSA/anti-CRP/ZnO/MPC/IL-CPE	DPV	0.005 (ng·mL^{-1})	0.01–1000 (ng·mL^{-1})	Dong et al. (2019a,b)
AuNPs/SPGE	DPV	1.5 (ng/mL)	0.01 × 10^3-150 × 10^3 (ng/mL)	Jampasa et al. (2018)
Au electrode with an aptamer	EIS	7.2 (pM)	10-5000 (pM)	Piccoli et al. (2018)
Metal–organic frameworks nanomaterials as novel signal probes	DPV	0.2 (ng/mL)	1-400 (ng/mL)	Liu et al. (2016)
Aptasensor based on 2Dp-COFs	Photo-electrochemical Sensor	0.10 (ng/mL)	0.5–100 (ng/mL)	Zhang et al. (2019)
BSA/anti-CRP/MPA/Au substrate	SWV	2.25 (fg/mL)	5 to 220 (fg/mL)	This work

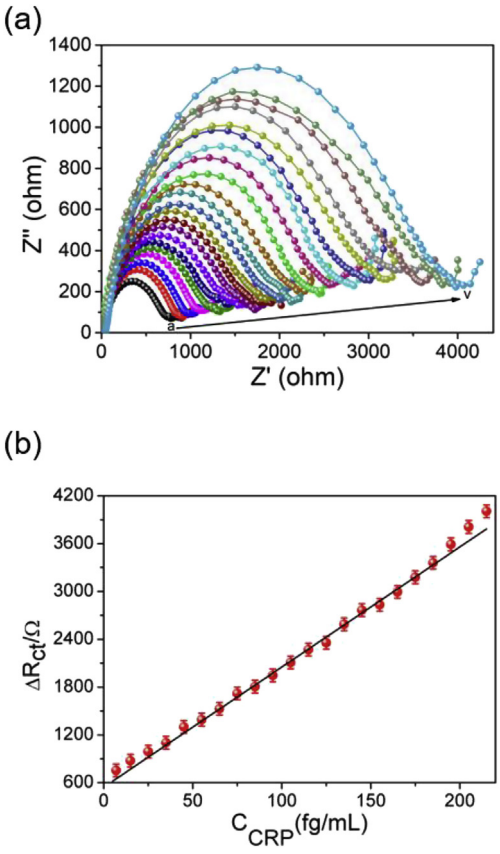

Fig. 5. (a) EIS response of electrochemical immunoassay with CRP concentration ranging from 7 to 215 pg/mL CRP (a to v, respectively), (b) Calibration plot of R_{ct} vs. concentration of CRP (n = 3).

characteristics (i.e., high sensitivity, a wide range of detection, and a LOD).

Furthermore, in this system, the analytical suitability of the CRP/BSA/anti-CRP/MPA/Au substrates was applied to the measurement of CRP in human saliva. The saliva was diluted 10-fold with 0.1 M PBS (pH 7.0), and serum samples were prepared by adding various concentrations of CRP (Fig. S9d). In the calibration plot, the R_{ct} value increases with CRP concentrations within the concentration range between 8 and 140 fg/mL and were related through linear segments described by $\Delta R_{ct} = 11.782x + 570.86$ (correlation coefficient: 0.9906; see Fig. S9d). These results indicate that the highly sensitive (detection limit of 4 fg/mL at an S/N value of 3), selective, and label-free CRP immunosensor is readily applicable to the diagnosis of CRP. All real sample experiments were performed three times and are independent. For the SWV and EIS calibration curve, the data were plotted by standard deviation method with error bars represent the standard deviation of the data. The respective data values are presented in Tables S8–S9.We believe that the excellent electrochemical activity of the BSA/anti-CRP/MPA/Au immunosensor can be mainly attributed to the good electron transfer nature of Au wires and their specific wire-like nanostructure, which offer an excellent micro-environment for immobilizing the CRP and anti-CRP resulting in the enhancement of electrochemical signal.

The reproducibility of the CRP/BSA/anti-CRP/MPA/Au substrate was also evaluated. A relative standard deviation (RSD) of 3.12% was obtained for CRP (14 fg/mL) detection of the six indistinguishable CRP/BSA/anti-CRP/MPA/Au substrate samples prepared under the same conditions (Fig. S10). This indicated that the CRP biosensor exhibits satisfactory reproducibility. Furthermore, the repeatability of the sensor was evaluated by six successive measurements with RSD of < 1.28% in the determination of CRP solution (14 fg/mL) using CRP/BSA/anti-CRP/MPA/Au substrate (Fig. S11) and the results indicate that this technique is suitable for the analysis of the drug quality control in biological fluids. The results revealed the excellent repeatability of the electrode and an RSD of < 1.28%, indicating that this technique is suitable for the routine analysis of the drug quality control in biological fluids. The stability of the immunosensor was also examined by recording SWV for the BSA/anti-CRP/MPA/Au substrate capturing CRP (14 fg/mL) over 30-day, which yielded an RSD of 3.68% (Fig. S12). After 30 days of storage under dry conditions in a refrigerator at 4 °C, the retained sensor response corresponded to 82.6% of the initial current. Morever, the proposed CRP biosensor exhibited good regeneration property and could be used repeatedly (i.e., at least six times) for CRP detection (Fig. S13). Good precision was realized for the CRP assay, as evidenced by intra-assay RSD values of < 3.82%. The aforementioned results all confirmed that the CRP/BSA/anti-CRP/MPA/Au substrate exhibits adequate reproducibility and long-term stability, rendering this substrate attractive for the fabrication of biosensors.

4. Conclusions

We developed a highly selective, label-free, and non-invasive ultrasensitive electrochemical immunosensor platform based on a BSA/anti-CRP/MPA/Au substrate for early-stage detection of cardiac failure biomarkers associated with CRP in human serum samples. The introduction of Au to the electrode PC substrate surface helped to enhance the ionic and electrical conductivities of the immunosensor and efficiently accelerated electron transfer and improved the electrochemical detection signal. The excellent performance of the immunosensor may be attributed to the excellent conductivity, the biocompatible microenvironment of the biomolecules, and large specific surface area of the Au substrate. A comparison of the present electrode with other substrate electrodes revealed the superior CRP sensing ability of our designed BSA/anti-CRP/MPA/Au substrate. The results also indicated the importance of nano-bio interface design in optimizing the performance of biosensors in general. Importantly, this new BSA/anti-CRP/MPA/Au substrate approach yielded highly sensitive

and selective detection of CRP over an extensive range (5–220 fg/mL) and a detection limit of 2.25 fg/mL. Therefore, this substrate ensures the reliable detection of CRP biomarkers of inflammation or cardiovascular diseases in clinical practice. The sensing performance (e.g., level of specificity, precision, and stability) was investigated. By exploiting the well-defined and amplified electrochemical signal of the Au nanowire-based network architecture, the results of this study should be helpful for the fabrication of novel electrochemical biosensors. This can be achieved by marrying the architecture to specific receptors for detecting other cancer types, and only requires samples from bodily fluids such as saliva, blood, and urine for the detection of cancer-specific biomarkers.

CRediT authorship contribution statement

A.T. Ezhil Vilian: Conceptualization, Formal analysis, Methodology, Writing - original draft, Supervision. **Wonyoung Kim:** Conceptualization, Data curation. **Bumjun Park:** Software, Project administration, Validation, Visualization. **Seo Yeong Oh:** Formal analysis, Funding acquisition, Investigation, Methodology. **TaeYoung Kim:** Methodology, Project administration, Funding acquisition. **Yun Suk Huh:** Conceptualization, Investigation, Visualization, Writing - review & editing, Supervision. **Chang Kwon Hwangbo:** Methodology, Investigation, Writing - review & editing, Supervision. **Young-Kyu Han:** Conceptualization, Writing - review & editing, Supervision.

Acknowledgments

We acknowledge financial support from the Basic Science Research Program through the National Research Foundation of Korea funded by the Ministry of Science, ICT & Future Planning (2019R1C1C1010306, 2017M2A2A6A01020938, 2016R1D1A1A09919495, and 2014R1A5A1009799).

Appendix A. Supplementary data

Supplementary data to this article can be found online at https://doi.org/10.1016/j.bios.2019.111549.

References

Baik, S., Zhang, H., Kim, Y.K., Harbottle, D., Lee, J.W., 2017. RSC Adv. 7 (86), 54546–54553.
Bryan, T., Luo, X., Bueno, P.R., Davis, J.J., 2013. Biosens. Bioelectron. 39 (1), 94–98.
Cai, Y., Kang, K., Liu, Y., Wang, Y., He, X., 2018. Anal. Biochem. 556, 129–135.
Cheen, O.C., Gopinath, S.C., Perumal, V., Arshad, M.M., Lakshmipriya, T., Chen, Y., Haarindraprasad, R., Rao, B.S., Hashim, U., Pandian, K., 2017. Microchim. Acta 184 (1), 117–125.
Chen, X., Wang, Y., Zhou, J., Yan, W., Li, X., Zhu, J.-J., 2008. Anal. Chem. 80 (6), 2133–2140.
Chen, Y.-S., Wu, C.-C., Tsai, J.-J., Wang, G.-J., 2012. Int. J. Nanomed. 7, 133.
Chen, Y., Lu, S., Zhang, S., Li, Y., Qu, Z., Chen, Y., Lu, B., Wang, X., Feng, X., 2017. Sci. Adv. 3 (12), e1701629.
Dong, S., Zhang, D., Cui, H., Huang, T., 2019a. Sens. Actuators B284, 354–361.
Dong, S., Cui, H., Zhang, D., Tong, M., 2019b. J. Electrochem. Soc. 166 (4), B193–B199.
Dorraki, M., Fouladzadeh, A., Salamon, S.J., Allison, A., Coventry, B.J., Abbott, D., 2018. Sci. Rep. 8 (1), 11979.
Gupta, R.K., Periyakaruppan, A., Meyyappan, M., Koehne, J.E., 2014. Biosens. Bioelectron. 59, 112–119.
Hu, W.-P., Hsu, H.-Y., Chiou, A., Tseng, K., Lin, H.-Y., Chang, G.-L., Chen, S.-J., 2006. Biosens. Bioelectron. 21 (8), 1631–1637.
Hühn, J., Carrillo-Carrion, C., Soliman, M.G., Pfeiffer, C., Valdeperez, D., Masood, A., Chakraborty, I., Zhu, L., Gallego, M., Yue, Z., 2016. Chem. Mater. 29 (1), 399–461.
Im, Y., Lee, C., Vasquez, R.P., Bangar, M.A., Myung, N.V., Menke, E.J., Penner, R.M., Yun, M., 2006. Small 2 (3), 356–358.
Jampasa, S., Siangproh, W., Laocharoensuk, R., Vilaivan, T., Chailapakul, O., 2018. Talanta 183, 311–319.
Jarczewska, M., Rębiś, J., Górski, Ł., Malinowska, E., 2018. Talanta 189, 45–54.
Johari-Ahar, M., Rashidi, M.R., Barar, J., Aghaie, M., Mohammadnejad, D., Ramazani, A., Karami, P., Coukos, G., Omidi, Y., 2015. Nanoscale 7 (8), 3768–3779.
Johnson, P.A., Gaspar, M.A., Levicky, R., 2004. J. Am. Chem. Soc. 126 (32), 9910–9911.
Kim, W., Hwang, S., Kim, T.Y., Ham, W.G., Kim, S., Lee, M., Hwangbo, C.K., 2018. Sci. Adv. Mater. 10 (5), 660–664.
Kim, W., Kim, M., Kim, T.Y., Choi, H., Jin, M.-J., Lee, K.-T., Lee, M., Hwangbo, C.K., 2019. Sci. Rep. 9, 4201.
Kitayama, Y., Takeuchi, T., 2014. Anal. Chem. 86 (11), 5587–5594.
Kokkinos, C., Prodromidis, M., Economou, A., Petrou, P., Kakabakos, S., 2015. Anal. Chim. Acta 886, 29–36.
Kowalczyk, A., Sęk, J.P., Kasprzak, A., Poplawska, M., Grudzinski, I.P., Nowicka, A.M., 2018. Biosens. Bioelectron. 117, 232–239.
Kuo, Y.-C., Lee, C.-K., Lin, C.-T., 2018. Biosens. Bioelectron. 103, 130–137.
Lakhtakia, A., Messier, R., 2005. Sculptured Thin Films: Nanoengineered Morphology and Optics. SPIE Press.
Lee, Y., Garcia, M.A., Frey Huls, N.A., Sun, S., 2010. Angew. Chem. 122 (7), 1293–1296.
Lee, W.-B., Chen, Y.-H., Lin, H.-I., Shiesh, S.-C., Lee, G.-B., 2011. Sens. Actuators B157 (2), 710–721.
Lee, H.-S., Seong, T.-Y., Kim, W.M., Kim, I., Hwang, G.-W., Lee, W.S., Lee, K.-S., 2018. Sens. Actuators, B 266, 311–317.
Lemos, A.J.G., Balvedi, R.P.A., Rodovalho, V.R., Resende, L.O., Castro, A.C.H., Cuadros-Orellana, S., Madurro, J.M., Brito-Madurro, A.G., 2017. Microchem. J. 133, 572–576.
Letchumanan, I., Md Arshad, M.K., Balakrishnan, S.R., Gopinath, S.C.B., 2019. Biosens. Bioelectron. 130, 40–47.
Li, Q., Liu, D., Xu, L., Xing, R., Liu, W., Sheng, K., Song, H., 2015. ACS Appl. Mater. Interfaces 7 (40), 22719–22726.
Liu, T.-Z., Hu, R., Zhang, X., Zhang, K.-L., Liu, Y., Zhang, X.-B., Bai, R.-Y., Li, D., Yang, Y.-H., 2016. Anal. Chem. 88 (24), 12516–12523.
Liu, Q., Yang, T., Ye, Y., Chen, P., Ren, X., Rao, A., Wan, Y., Wang, B., Luo, Z., 2019. J. Mater. Chem. B 7 (9), 1442–1449.
Matsuura, R., Tawa, K., Kitayama, Y., Takeuchi, T., 2016. Chem. Commun. 52 (20), 3883–3886.
McAlpine, M.C., Ahmad, H., Wang, D., Heath, J.R., 2007. Nat. Mater. 6 (5), 379.
Mohammed, M.-I., Desmulliez, M.P., 2011. Lab Chip 11 (4), 569–595.
Piccoli, J., Hein, R., El-Sagheer, A.H., Brown, T., Cilli, E.M., Bueno, P.R., Davis, J.J., 2018. Anal. Chem. 90 (5), 3005–3008.
Salminen, K., Grönroos, P., Eskola, J., Nieminen, E., Härmä, H., Kulmala, S., 2018. Electrochim. Acta 282, 147–154.
Songjaroen, T., Feeny, R.M., Mensack, M.M., Laiwattanapaisal, W., Henry, C.S., 2016. Sens. Bio. Sens. Res. 8, 14–19.
Suginta, W., Khunkaewla, P., Schulte, A., 2013. Chem. Rev. 113 (7), 5458–5479.
Sun, Y., Gates, B., Mayers, B., Xia, Y., 2002. Nano Lett. 2 (2), 165–168.
Thangamuthu, M., Santschi, C., JF Martin, O., 2018. Biosensors 8 (2), 34.
Thapliyal, N., Chiwunze, T.E., Karpoormath, R., Goyal, R.N., Patel, H., Cherukupalli, S., 2016. RSC Adv. 6 (62), 57580–57602.
Thurn-Albrecht, T., Schotter, J., Kästle, G., Emley, N., Shibauchi, T., Krusin-Elbaum, L., Guarini, K., Black, C., Tuominen, M., Russell, T., 2000. Science 290 (5499), 2126–2129.
Turner, A.P., 2013. Chem. Soc. Rev. 42 (8), 3184–3196.
Vashist, S.K., Venkatesh, A.G., Marion Schneider, E., Beaudoin, C., Luppa, P.B., Luong, J.H.T., 2016. Biotechnol. Adv. 34 (3), 272–290.
Vigushin, D.M., Pepys, M.B., Hawkins, P.N., 1993. J. Clin. Investig. 91, 1351–1357.
Vilian, A.T.E., Dinesh, B., Kang, S.-M., Krishnan, U.M., Huh, Y.S., Han, Y.-K., 2019. Microchim. Acta 186 (3), 203.
Wang, Y., Li, X., Cao, W., Li, Y., Li, H., Du, B., Wei, Q., 2014. Biosens. Bioelectron. 61, 618–624.
Wang, J., Guo, J., Zhang, J., Zhang, W., Zhang, Y., 2017a. Biosens. Bioelectron. 95, 100–105.
Wang, Y.-H., Huang, K.-J., Wu, X., 2017b. Biosens. Bioelectron. 97, 305–316.
Wongkaew, N., Simsek, M., Griesche, C., Baeumner, A.J., 2018. Chem. Rev. 119 (1), 120–194.
Xie, P., Xiong, Q., Fang, Y., Qing, Q., Lieber, C.M., 2012. Nat. Nanotechnol. 7 (2), 119.
Xing, Y., Xi, Z., Xue, Z., Zhang, X., Song, J., Wang, R., Xu, J., Song, Y., Zhang, S., Yu, D., 2003. Appl. Phys. Lett. 83 (9), 1689–1691.
Yeon, J., Lee, Y.J., Yoo, D.E., Yoo, K.J., Kim, J.S., Lee, J., Lee, J.O., Choi, S.-J., Yoon, G.-W., Lee, D.W., 2013. Nano Lett. 13 (9), 3978–3984.
Yuan, X., Choi, S.W., Jang, E., Lee, K.B., 2018. Chem. Eng. Sci. 336, 297–305.
Zamay, G.S., Zamay, T.N., Kolovskii, V.A., Shabanov, A.V., Glazyrin, Y.E., Veprintsev, D.V., Krat, A.V., Zamay, S.S., Kolovskaya, O.S., Gargaun, A., Sokolov, A.E., Modestov, A.A., Artyukhov, I.P., Chesnokov, N.V., Petrova, M.M., Berezovski, M.V., Zamay, A.S., 2016. Sci. Rep. 6, 34350.
Zhang, X., Hu, R., Zhang, K., Bai, R., Li, D., Yang, Y., 2016. Anal. Methods 8 (32), 6202–6207.
Zhang, J., Zhang, W., Guo, J., Wang, J., Zhang, Y., 2017. Anal. Biochem. 539, 1–7.
Zhang, X., Chi, K.-N., Li, D.-L., Deng, Y., Ma, Y.-C., Xu, Q.-Q., Hu, R., Yang, Y.-H., 2019. Biosens. Bioelectron. 129, 64–71.
Zhou, F., Lu, M., Wang, W., Bian, Z.-P., Zhang, J.-R., Zhu, J.-J., 2010. Clin. Chem. 56 (11), 1701–1707.
Zhou, J., Tang, J., Chen, G., Tang, D., 2014. Biosens. Bioelectron. 54, 323–328.
Zubiate, P., Zamarreño, C., Sánchez, P., Matias, I., Arregui, F., 2017. Biosens. Bioelectron. 93, 176–181.